Influence on donor electron energies of the chemical composition of K, Na and Ca aluminosilicates

1995 J. Phys.: Condens. Matter 7 4751

(http://iopscience.iop.org/0953-8984/7/24/014)

J. Phys.: Condens. Matter 7 (1995) 4751–4762. Printed in the UK

Influence on donor electron energies of the chemical composition of K, Na and Ca aluminosilicates

N R J Poolton†, L Bøtter-Jensen† and O Johnsen‡

† Risø National Laboratory, DK-4000 Roskilde, Denmark

‡ Geological Museum, University of Copenhagen, DK-1350 Copenhagen, Denmark

Received 28 July 1994, in final form 14 March 1995

Abstract. The chemical composition of $K_xNa_{1-x}AlSi_3O_8$ and $Na_yCa_{1-y}Al_{2-y}Si_{2+y}O_8$ crystals (alkali and plagioclase feldspars) is shown to determine the optical transition energies of electrons trapped at donor centres within them. Optical resonances in the infrared region 1.2–1.5 eV can be interpreted as arising from the 1s–2p transition of an ideal Bohr hydrogen donor. Shifts in the energy positions with sample composition are well accounted for by variations in the dielectric constant. Within the context of the Bohr model, the effective electron mass and donor radii can be determined. The mass is found to be $0.76m_e$ in the K–Na series but slightly higher, at $0.79m_e$ in $CaAl_2Si_2O_8$. The ground-state donor radii are determined as 1.62 Å, 1.63 Å and 1.68 Å in the K, Na and Ca end members, respectively; these values closely match the mean (Si, Al_{Si})–O bond lengths in the material for tetrahedra with mean Al content.

1. Introduction

The wide-band-gap insulators $K_xNa_{1-x}AlSi_3O_8$ and $Na_yCa_{1-y}Al_{2-y}Si_{2+y}O_8$ (more commonly referred to as alkali and plagioclase feldspars, respectively) are the most abundant minerals in the Earth's crust; they constitute the major part of virtually all igneous rocks, and they often form a significant proportion of metamorphic and sedimentary rocks. The minerals are often luminescent, and a study of their emission properties can be used as a tool for monitoring the presence of certain impurities, their charge states and defect structures. More practically, the materials can be used as naturally occurring radiation dosemeters, and their ubiquitous distribution has obvious advantages for radiation dose assessment in areas of accidental nuclear contamination, or dating studies. In such measurements, radiation-induced charge becomes trapped at certain lattice defects, stable over long periods of time, and the accumulated dose may be monitored by thermally stimulated luminescence (TL) and optically stimulated luminescence (OSL) techniques (see, e.g., Aitken (1985), Hütt *et al* (1988), Duller (1991) and Wintle (1993)).

For both TL and OSL measurements, the presence of charge located at both donor and acceptor centres is required; during stimulation, the charge is transferred from one defect to the other, giving rise to the luminescence emission. When present, the transition-metal impurities Fe^{3+} and Mn^{2+} may act as deep recombination centres (Prescott and Fox 1993), and their energy levels are well accounted for in terms of crystal-field theory (Manning 1970, Telfer and Walker 1978). In contrast, the nature and identity of the OSL donor defects are poorly understood. A distinguishing feature of some of the OSL donors, reported by a number of workers (Hütt *et al* 1988, Bailiff 1993, Clark and Sanderson 1994, Bøtter-Jensen *et al* 1994a), is the presence of well defined optical transitions in the infrared region 1.2–1.7 eV; these were originally postulated to be internal transitions from the ground to the

0953-8984/95/244751+12$19.50

excited state of the donor defect (Hütt *et al* 1988), but neither the identity of the donor nor the reason for the excited state has been determined. When photoexcited to these states, electrons can escape from the centres with thermal assistance even at room temperature; this is an aspect that is commonly made use of in radiation dosimetry measurements (see, e.g., Bøtter-Jensen *et al* (1991)). It is interesting to contrast such behaviour with that of pure quartz, where no structure is observed in the excitation spectrum at room temperature, and the OSL emission intensity simply rises exponentially with increasing photon excitation energy (Bøtter-Jensen *et al* 1994a).

It is the intention of this article to present new experimental data concerning the optical transitions of donor centres over the full composition range of the feldspars, and to provide a model that accounts for both the presence of the infrared transitions, and the variation in their energy positions within the K–Na–Ca feldspar group. Since the identity of neither the donor nor the electronic transitions is known, establishing such a model is problematic, and we have little choice at this stage but to consider the simplest possible situations. It is possible, however, to draw some analogy with the classic F centres in alkali halides; these are probably the best understood and simplest of lattice defects (a cation vacancy in a cubic lattice). F centres typically show a single, well defined absorption band below their photo-ionization energy; when present, the F centre absorption is directly coincident with a peak in the OSL excitation spectra (see, e.g., Kalniņš *et al* (1991)). Earlier work (summarized by Fowler (1968)) sought to account for the electronic energy levels of the F centre donors in terms of either the simple Bohr hydrogen model or as an electron in a 3D square-well potential ('particle in a box'). It is shown in this article that the Bohr hydrogen model works particularly well in feldspars and, in this context, the observed OSL resonances in the infrared region are interpreted as arising from the 1s–2p transition of the centre. The use of the model does suggest that the OSL donor is a simple point defect, possibly a lattice vacancy. Finally, the interpretation of the results also provides some information regarding the K–Na–Ca mixing on a submicroscopic scale.

2. Experimental details

2.1. Samples, structure and composition

35 samples of the ternary feldspar system were loaned from the Mineral Collection of the Geological Museum, University of Copenhagen. X-ray powder diffraction was used to determine the structural state of these samples via the method given by Wright and Stewart (1968) and Kroll and Ribbe (1983), whilst electron microprobe analysis was used in most cases to determine the chemical composition. Each sample was checked for chemical homogeneity and, where necessary, the homogeneity was observed over the analysed area by making back-scattered electron images. The spatial resolution of the microprobe is expressed in terms of a bulb-shaped volume of approximately 10^{-16} m^3 with a surface area of about 10^{-11} m^2.

Feldspars rapidly cooled from the melt preserve a random mixture of Ca, Na and K on crystallization and would be closest to a pure alloy of the material (the 'high-temperature' form); for analysing the luminescence data, spectra from these samples would be the easiest to interpret. Significantly, nearly all the samples actually showing OSL strong enough to analyse were found to be 'low-temperature' forms, i.e. samples that had been slowly cooled; here, miscibility gaps can arise owing to cation ordering, giving rise to exsolution textures in the crystals on macroscopic, microscopic or submicroscopic scales. There is considerable difference in the nature of these exsolution textures, depending on whether the

$K_xNa_{1-x}AlSi_3O_8$ (alkali feldspar) or $Na_yCa_{1-y}Al_{2-y}Si_{2+y}O_8$ (plagioclase feldspar) series are monitored. (It should be noted that there is virtually no mixing between $KAlSi_3O_8$ and $CaAl_2Si_2O_8$, so that only the two series need be considered.) For the Na–K alkali feldspar series described in this article, exsolution into almost pure Na- and K-rich phases was found to occur on scales larger than 1 μm, as can be seen in figure 1; this probably occurs because K^+ and Na^+ are isoelectronic, and minimum energy is required for the cation ordering. In contrast, ordering in the plagioclase $Na_yCa_{1-y}Al_{2-y}Si_{2+y}O_8$ series requires the coupled substitution $(Na^+ + Si^{4+}) \rightleftharpoons (Ca^{2+} + Al^{3+})$, which can only be made by major reconstruction of the lattice; in all the samples of this series studied here, any exsolution textures present were on a scale smaller than the resolution of the microprobe and were thus not observable.

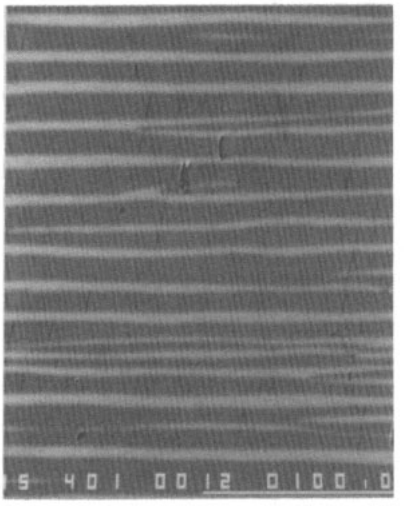

Figure 1. Electron micrograph of sample R34. The figure demonstrates the exsolution into lamellae of Na-rich and K-rich phases of the material (dark and light bands, respectively). The scale is shown by the bar in the bottom right-hand corner (100 μm).

The 35 feldspar samples were initially selected for study, such that their bulk compositions covered the full range of both feldspar groups. Although most of these showed some OSL, only 18 gave signals that were strong enough to allow their excitation characteristics to be established. Of these 18 samples, only 12 were found to be homogeneous on the scale of the microprobe (table 1). The remaining samples, exclusively from the Na–K alkali feldspar series, showed well resolved intergrowth zones of the type shown in figure 1; the compositions of both phases in these samples are given in table 2, where the dominant phases are indicated.

Finally in this section, a comment is made on the accuracy of the chemical compositions given in tables 1 and 2. The microprobe analyses are an average of between two and eight measurements, and the amount of each element present is assessed by reference to different chemical standards (wollastonite, orthoclase and albite). It will thus be apparent that the total K + Na + Ca content does not always sum to 1.00; for the homogeneous samples, the difference is typically 2%. Because of the scarcity of sample R23, the composition was determined directly from the XRD data (for the method, see Wright and Stewart (1968)); this sample is close to pure $CaAl_2Si_2O_8$, and the Ca content was determined to $\pm 4\%$. However, since it is not possible to determine the ratio of the small remaining amount of Na and K directly, these values are not included in table 1.

Table 1. Structures, compositions and OSL data for feldspar samples observed to be homogeneous on the scale of the microprobe (see text for analysis procedures). The structure is given as low (L), intermediate (I) or high (H). The OSL data show the energy positions $E(1)$ and $E(2)$ of the deconvoluted peaks, their widths $W(1)$ and $W(2)$ (HWHM) and relative intensities $I(1)$ and $I(2)$.

		Composition			Peak energy (eV)		Peak width (eV)		Peak relative intensity	
Sample	Structure	K	Na	Ca	$E(1)$	$E(2)$	$W(1)$	$W(2)$	$I(1)$	$I(2)$
R35	L	0.99	0.02	0.00	1.430	—	0.085	—	100	—
R28	I	0.95	0.05	0.00	1.440	—	0.090	—	100	—
R13	L	0.67	0.33	0.01	1.438	1.43	0.080	0.16	100	11
R25	I	0.23	0.76	0.05	1.435	—	0.085	—	100	—
R29	L	0.00	0.99	0.01	1.423	—	0.104	—	100	—
R12	L	0.01	1.01	0.01	1.422	—	0.104	—	100	—
R27	L	0.01	0.92	0.07	1.415	1.30	0.108	0.08	100	6
R38	L	0.01	0.87	0.12	1.412	1.28	0.107	0.08	100	7
R37	L	0.00	0.79	0.21	1.415	1.30	0.108	0.08	100	10
R8	L	0.01	0.71	0.26	1.410	—	0.115	—	100	—
R5	L	0.02	0.57	0.39	1.420	1.28	0.104	0.08	100	23
R23	L–H	(—	—	0.9)	1.38	1.275	0.09	0.080	55	100

Table 2. Structures, compositions and OSL data for alkali feldspar samples observed to have segregation lamellae on a scale larger than that of the microprobe. The composition of both phases is given. M denotes the main host lattice type. Other symbols are the same as in table 1. Both crystal phases are excited in the measurements.

		Composition			Peak energy (eV)		Peak width (eV)		Peak relative intensity	
Sample	Structure	K	Na	Ca	$E(1)$	$E(2)$	$W(1)$	$W(2)$	$I(1)$	$I(2)$
R19	M	0.99	0.03	0.00	1.410	—	0.130	—	100	—
		0.01	1.06	0.01						
R20	M	0.98	0.02	0.00	1.424	1.31	0.088	0.08	100	8
		0.01	1.01	0.03						
R36	M	0.98	0.04	0.00	1.430	1.30	0.085	0.08	100	7
		0.02	0.98	0.01						
R7	M	0.97	0.04	0.00	1.415	1.28	0.098	0.08	100	17
		0.01	0.97	0.01						
R18	M	0.96	0.06	0.00	1.418	1.30	0.090	0.08	100	7
		0.01	1.03	0.03						
R34	M	0.03	0.96	0.02	1.420	—	0.104	—	100	—
		0.97	0.04	0.00						

2.2. Luminescence measurements

All the luminescence measurements were made at room temperature on crystals with freshly cleaved surfaces, typically of dimensions 2 mm × 2 mm × 1 mm. As OSL is an ionizing-radiation-dose-dependent signal, samples were irradiated prior to measurement using the β emission from a Sr^{90} source. Doses administered were in the range 50–200 Gy, well below the saturation limit where shifts in the spectra might be expected owing to interaction between closely spaced defect pairs. As excitation of the donor centres occurs at a lower energy than the emission wavelengths of the acceptor centres, luminescence was stimulated in the infrared region (750–1000 nm; 1.24–1.65 eV) and detected in the visible and near UV (350–600 nm; 2.1–3.5 eV). Monochromatic excitation was made using a Risø-built monochromator (Bøtter-Jensen *et al* 1994b) with resolution set to 15 nm throughout, coupled to a 75 W incandescent tungsten–halogen lamp. Broad-band detection was made using

3 mm of standard Schott BG39 filter (transmission range, 350–600 nm) in conjunction with a blue-sensitive photomultiplier tube (EMI 9635QB) in photon-counting mode. The excitation spectra are corrected for the instrumental response of the system in terms of incident number of photons per unit energy (equivalent to correcting for incident power per unit wavelength).

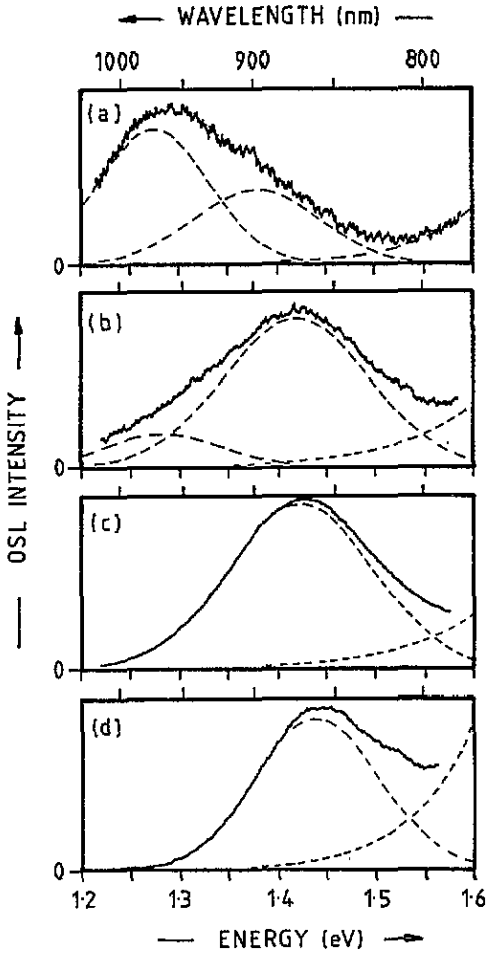

Figure 2. The infrared OSL transitions (at 300 K), for four typical samples of irradiated feldspar: (a) R23 ($y = 0.1$); (b) R5 ($y = 0.57$); (c) R12 ($x = 0.01$); (d) R28 ($x = 0.95$). Curve fitting establishes the parameters of the main components of the signals (shown here by the broken lines); these consist of a featureless background, increasing at higher energy, and either one or two Gaussian bands. The OSL intensity is in photon counts, and corrected for incident number of photons per unit energy.

3. Results and discussion

3.1. General characteristics

Shown in figure 2 are the luminescence excitation characteristics obtained in a

representative selection of samples in the two feldspar series $Na_yCa_{1-y}Al_{2-y}Si_{2+y}O_8$ and $K_xNa_{1-x}AlSi_3O_8$, such that $y = 0.10$ and 0.57 (samples R23 and R5, respectively, and $x = 0.01$ and 0.95 (samples R12 and R28, respectively). It is evident from figure 2 that the spectra do not always consist of a single transition; curve fitting has been used to determine the peak positions, widths and intensities of the poorly resolved components. In most cases, satisfactory fits to the data could be produced be considering either one or two Gaussian transitions (in energy terms), together with a component increasing exponentially in intensity with increasing energy, used to approximate for the rising continuum dominant in the visible range. The latter is not considered further in this study. The reason why the lineshapes are Gaussian and not Lorentzian possibly arises from either thermal broadening effects or, more probably, site-to-site variations in the crystal environment of the defects distributed throughout the samples.

The results of the curve fitting, giving the position, linewidths and relative intensities for the 18 samples, are given in tables 1 and 2. Table 1 gives the data for the samples that were found to have uniform composition on the scale of the microprobe, and these results form the basis of the analysis given in the following sections. The results presented in table 2 are those of the segregated K–Na alkali feldspars.

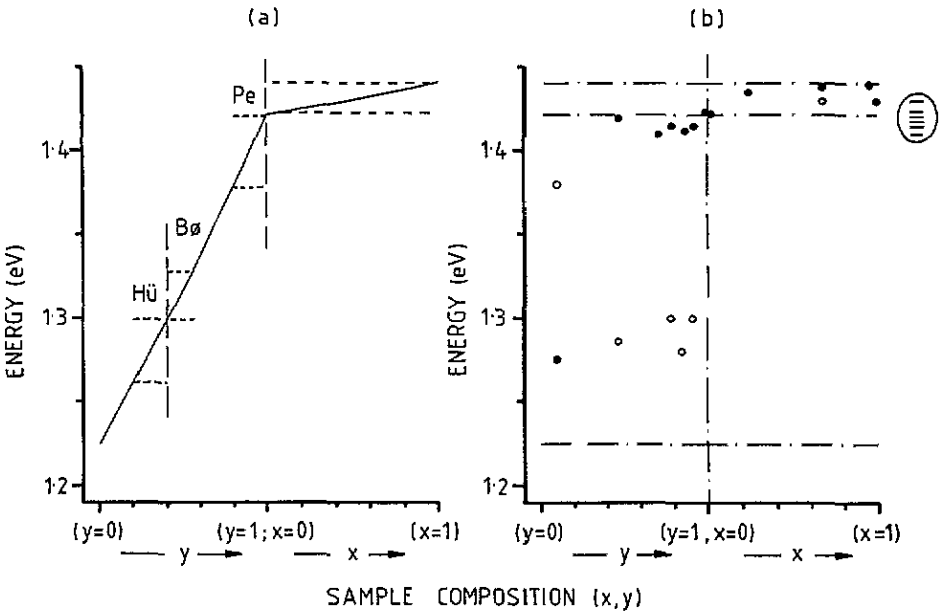

Figure 3. (a) OSL transition energies in $K_xNa_{1-x}AlSi_3O_8$ and $Na_yCa_{1-y}Al_{2-y}Si_{2+y}O_8$ as determined from the hydrogenic model. The solid line is for a pure alloy system, and the horizontal broken lines are for samples displaying exsolution textures (as in figure 1). The three regions indicated are the common segregation zones: (Pe, peristerite; Bøggild, Bø; Hü, Hüttenlocher. See text for details. (b) Experimentally determined data, taken from table 1. The full circles are the main peaks; the open circles are weaker components. The horizontal lines delimit the calculated energies of the end members. To the right of the diagram in the ellipse, the positions of the main signals are shown for data taken from table 2.

The overall features of the OSL in the ternary system can best be appreciated by reference to figure 3(b), where the results of table 1 are plotted. The general shift in the peak position

on moving from K- to Na- to Ca-rich material is clear but, while the energies change only a small amount between the end members of the Na–K alkali feldspar group, a much larger overall shift in the Na–Ca group is noticeable. Of significance is that, where samples are almost exactly representative of the Na–K end members, only single OSL transitions are observed, whereas double transitions are seen in samples of intermediate compositions in the Na–Ca feldspar group. We also note here that the component transition bandwidths are smallest in the K-rich materials and are considerably larger in the Na–Ca-rich samples (HWHM typically 0.08 eV in $KAlSi_3O_8$, and 0.10 eV in $NaAlSi_3O_8$).

Since the peak positions (and energy widths) of the OSL transitions have been determined via curve fitting, it is important to comment on the accuracy of the energies thus determined. Neglecting systematic errors of experimental measurement, the energy position in any individual sample can normally be determined to three significant figures (typically ± 0.04 eV). However, the energy positions can only be taken to two significant figures when the systematic errors of experimental measurement are also taken into account (typically ± 0.01 eV); these systematic errors are not important here when comparing the *change* in energy from one sample to another. Similar arguments holds for the accuracy of the effective masses used which, it is emphasized, are derived from the Bohr model and determined using the measured OSL peak positions.

3.2. The Bohr hydrogen model: $KAlSi_3O_8$, $NaAlSi_3O_8$ and $CaAl_2Si_2O_8$

The intention here is to show that optical transitions within the donor defects that give rise to the OSL resonances can be regarded in analogy with the hydrogen atom. In the Bohr hydrogen model, the energy and radius of the nth level below the ionization level (conduction band in this case) are given by the familiar expressions (see, e.g., Fowler (1968))

$$E_n = \frac{-E_h(m^*/m_e)}{(\epsilon_r n)^2} \qquad R_n = \frac{R_h n^2 \epsilon_r}{m^*/m_e}$$

where E_h (= 13.6 eV) and R_h (= 0.53 Å) are the ionization energy and Bohr radius of free hydrogen, m^* is the effective mass of the electron in the lattice, m_e is the electron rest mass and ϵ_r is the relative permittivity of the host crystal.

The relative permittivities of the feldspars are well documented. Keller (1966) shows a nearly linear change across the $Na_yCa_{1-y}Al_{2-y}Si_{2+y}O_8$ series from 2.33 ($y = 0.99$) to 2.51 ($y = 0.02$), apart from a slightly sublinear region between $y = 1$ and $y = 0.95$. In $K_xNa_{1-x}AlSi_3O_8$, the values range between 2.33 ($x = 0$) and 2.32 ($x = 1$). The data presented by Deer *et al* (1992) are broadly the same, with values (taken as the square of the refractive index) ranging from 2.31 ($KAlSi_3O_8$) to 2.35 ($NaAlSi_3O_8$) to 2.51 ($CaAl_2Si_2O_8$). In the present work, values are taken that vary linearly between the limits 2.315, 2.330 and 2.510 for the K, Na and Ca end members, respectively.

To our knowledge, the effective masses of electrons in feldspars have neither been measured nor been calculated. However, it is unlikely that the mass will vary significantly with feldspar composition, and m^* should be smaller than m_e. Moreover, the value may be expected to be in the region of that determined for NaCl, 0.62 (Evseev 1964), or for SiO_2, 0.48 (Weinberg *et al* 1976). As a starting point for the discussion presented here, the value is taken such that $m^* = 0.757m_e$; this value is derived from the Bohr equation and is based on the energy position of the OSL resonance in the end-member sample (sample R12, $NaAlSi_3O_8$) where the energy difference between the ground state and the first excited state is 1.422 eV (with $\epsilon_r = 2.330$). This sample is chosen to evaluate m^*, since the $NaAlSi_3O_8$

is common to both the feldspar series and, furthermore, only a single OSL transition is discernible. The other pure $NaAlSi_3O_8$ sample in the collection, sample R29, yields the same value for m^*.

Based on the Bohr hydrogen model, the calculated positions of the 1s–2p transitions in K, Na and Ca end members are 1.441 eV, 1.422 eV and 1.225 eV, respectively, and these compare with the experimentally determined values of material *close* to the end members, namely 1.440 eV, 1.422 eV and 1.275 eV (samples R28, R12 and R23, resepectively). It will be evident that the simple model accounts for both the direction and the magnitude of the shift in the OSL transition energies in the two feldspar groups; the value of m^* may be marginally higher for Ca-rich material ($0.788m_e$) than for the Na–K samples ($0.757m_e$) and this possibility is discussed further in section 3.4.

3.3. Optical transitions in the full ternary system

3.3.1. Fully mixed samples. Since the Bohr hydrogen model was shown to work well in accounting for the OSL peak positions in the K, Na and Ca end-member samples, determining the expected OSL transition energy in the midrange samples is straightforward if a complete alloy system is assumed. This would be best represented by the 'high-temperature' series, where rapid cooling of the crystals from the melt retains a random arrangement of the cations. The OSL transitions would be expected to lie on the single continuous curve, as shown in figure 3(a) by the solid line; as a first approximation here, the effective electron mass has been taken to be constant for all sample compositions ($0.757m_e$), and the relative permittivities have been taken to change linearly between the end-member values.

There is very little evidence from the experimental data plotted in figure 3(b) that the above situation is representative of the main samples actually studied here, even though they were observed to have 'uniform' composition on the scale of the microprobe ($10^{-11}m^2$). The fact that most of the samples were low-temperature forms of the crystals provides a strong indication that there may be further exsolution and inhomogeneities on a much finer scale (see section 2.1). Certainly, the fact that double transitions are observed in the Na–Ca feldspar range is very good initial evidence for this.

3.3.2. Unmixed samples. In considering the effects of exsolution, both the crystal structure *and* the nature of the luminescence centres must be taken into account. One problem here is that, although the intention of this work is to determine the structure of the donor centres, this is done while monitoring the emission from other defects, the acceptors. For a crystal showing two exsolution phases (1 and 2), the characteristics are a combination of (E_1, λ_1) and (E_2, λ_2) where E and λ are the excitation energy and emission wavelength, respectively. Thus, if the detector does not detect a λ_1, or the excitation–emission efficiency of phase 1 is low, or the donor-acceptor defects are not present in phase 1, only the characteristics of phase 2 will be monitored. There is certainly some evidence for this type of behaviour from the experimental results. For the clearly exsolved Na–K feldspar samples (of the type shown in figure 1), the OSL excitation characteristics are almost invariably close to those of $NaAlSi_3O_8$, even where the K-rich component is the dominant phase; these data are plotted in the ellipse in figure 3(b).

The luminescence emission characteristics for the samples used in this study were not specifically determined, but generally (in the wavelength range of interest in our experiment, 350–600 nm) the Na–Ca plagioclase feldspars are dominated by the extrinsic impurity Mn^{2+} emission at around 560 nm whereas, in the alkali Na–K feldspars, emission changes from the 560 nm band in Na-rich material to that of an intrinsic lattice defect, emitting close to

400 nm in K-rich material (Telfer and Walker 1975, Huntley *et al* 1989, 1991, Prescott and Fox 1993).

In considering the possible effects of exsolution on the OSL excitation spectra, the two feldspar groups are considered separately, since they each have their own characteristics. In the Na–K alkali feldspar series, submicroscopic exsolution is most likely into material close to either end member. It will be apparent that, when both these phases are present (and luminescence is excitable), the individual OSL transitions would not be observed in our experiment, since the resolution is too low; the typical resonance linewidths are 0.09 eV (HWHM) compared with an expected difference in energy position of 0.02 eV. Since the detector collects luminescence emission from both phases, there is little surprise that the OSL peak energy simply shifts between two end-member energies (see figure 3(b)). Although this shift is systematic, there is more than expected scatter in the data, and this almost certainly arises (at least in part) from sample-to-sample variation in the emission characteristics or excitation efficiencies of the two components.

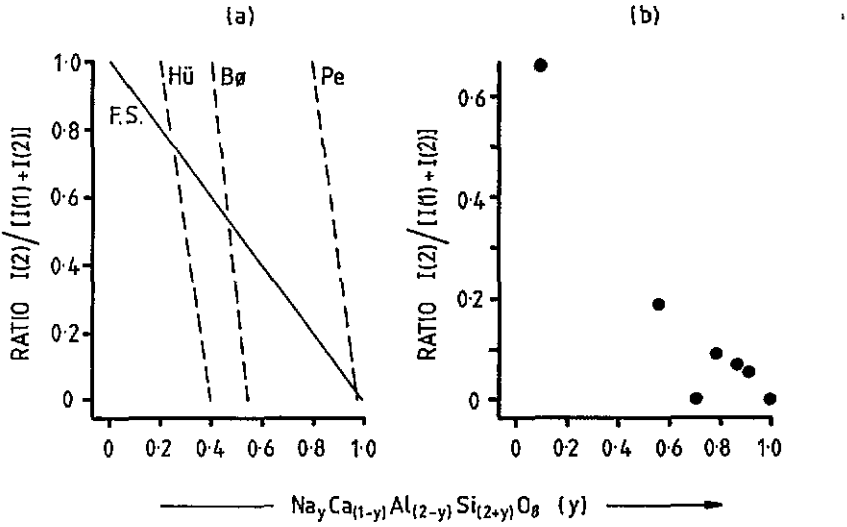

Figure 4. (a) The intensity ratio of the OSL transitions expected in low-temperature forms of the $Na_yCa_{1-y}Al_{2-y}Si_{2+y}O_8$ series, given that the defect concentations, emission and excitation efficiencies are the same for all phases present. The solid line is expected if exsolution into the pure $NaAlSi_3O_8$ and $CaAl_2Si_2O_8$ phases is complete (full segregation (FS)), the broken line is for partial exsolution within the main intergrowth zones. (b) The experimental results.

Predicting where the OSL transitions should occur in the midrange, the low-temperature $Na_yCa_{1-y}Al_{2-y}Si_{2+y}O_8$ plagioclase feldspar series is more complex, although the effects of differences in the emission wavelengths are smaller than for the Na–K series. Because coupled substitution is required for cation ordering, the submicroscopic exsolutions are usually only partial. Three types are normally identified (see, e.g. Deer *et al* (1992)), occurring in the ranges $y = 0.98$–0.8, $y = 0.55$–0.40 and $y = 0.40$–0.20, referred to as peristerite, Bøggild and Hüttenlocher intergrowths. *Within* the segregated regions, the average compositions are normally found to be close to the end members of the *intergrowth* (rather than the whole series). For example, the two lamellae in the Bøggild range would have $y = 0.55$ and $y = 0.40$ (and not $y = 0$ and $y = 1$). The positions of the OSL

resonances in the Na–Ca feldspar series would thus be expected to occur on the highly fragmented curve, as shown by the broken curve in figure 3(a). While being qualitatively closer to this situation than that of the pure alloy, the experimental data for the Na–Ca feldspar series still does not match the situation anticipated, since the component transitions are split in energy more than expected. This could be indicative that exsolution on the very finest scale (that of a few lattice cells surrounding the OSL donor effect) could be into zones of material much closer to the end-member compositions $NaAlSi_3O_8$ and $CaAl_2Si_2O_8$. More information can be gained on this aspect by considering the intensities of the two OSL transitions. Plotted in figure 4(a) are the expected ratios in the two limiting conditions: that of complete segregation into components $y = 0$ and $y = 1$ across the full composition range, and that where the regime of peristerite, Bøggild and Büttenlocher intergrowths occur into zones of ($y = 0.98, 0.8$), ($y = 0.55, 0.4$) and ($y = 0.4, 0.2$), respectively. It is not unreasonable to consider that the observed experimental results might lie somewhere between these two limiting conditions. The actual results (figure 4(b)) show a *continuous* shift in the relative intensities over the whole Na–Ca plagioclase feldspar composition range, partly confirming the possibility that exsolution is more complete on the very finest scale.

3.4. Donor radii and lattice spacings

Since the Bohr hydrogen model is shown to account well for the positions at which the OSL transitions are seen to occur (at least in the K-, Na- and Ca-rich materials), the same model is also used to consider the size of the donor radii. In the ground state, these will be 1.62 Å and 1.63 Å in $KAlSi_3O_8$ and $NaAlSi_3O_8$, respectively, and either 1.75 Å (if $m^* = 0.757m_e$) or 1.69 Å (if $m^* = 0.788m_e$) for $CaAl_2Si_2O_8$; these values are based on the equation given in section 3.2. The radii can be compared with the mean (Si, Al_{Si})–O bond lengths measured in the materials for tetrahedra with mean Al content; for the K, Na and Ca end members, these are 1.64 Å, 1.65 Å and 1.68 Å, respectively (Kroll and Ribbe 1983). The correspondence between the bond lengths and donor radii is remarkable; both the absolute magnitudes are similar, as is the trend of increasing distance on moving from K- to Na- to Ca-rich material. The values should be contrasted against the much larger interstitial–oxygen separations in the materials (typically between 2.7 and 3.3 Å). The result is a clear indication that the OSL defect is located at either an oxygen site or more probably a tetrahedrally coordinated Si site; furthermore, the defect is likely to be simple (rather than compound), since the electron wavefunction is so compact. In either case, a vacancy centre is an attractive possibility, confirming the earlier comparison with *F centres in alkali halides. It is noted here that in the Na–K alkali feldspars an absorption* band in the infrared region 1.41–1.44 eV has previously been assigned to charge trapped between Si non-bonding orbitals (Hofmeister and Rossman 1985), but further work will be required to confirm the identity of the OSL donor defect positively.

The above comments raise an issue that seems somewhat paradoxical. On the one hand, the simple Bohr model appears to work well both in explaining the positions of the OSL resonance in feldspars, and in yielding the donor radii that can be understood directly in terms of physically real quantities (the bond lengths). Conversely, it is somewhat surprising that the Bohr model *does* work when the electron orbit is so compact, since the effective electron mass is usually taken to refer to an electron moving through the continuum of the crystal (i.e. requiring a delocalized orbit). Comparison could be drawn with the hydrogen donor in silicon, for example (see, e.g., Kittel (1967)), where the donor radius for the ground state would be 30 Å ($m^* = 0.2m_e$; $\epsilon_r = 11.7$). At this stage, it is too premature to give an entirely satisfactory response to the apparent contradiction. However, one possible reason for the success of the Bohr model in the case of feldspar could lie in the fact that (m^*, ϵ) are

much closer to (m_e, ϵ_0) than in silicon, i.e. the feldspar lattice has a relatively small effect on the donor electron behaviour. Determination of m^* by other methods would certainly help to clarify the problem.

4. Concluding remarks

Two important conclusions arise from the work presented in this article: firstly, that the positions at which the infrared OSL donor transitions occur in $KAlSi_3O_8$, $NaAlSi_3O_8$ and $CaAl_2Si_2O_8$ is well accounted for in terms of the 1s–2p transition of the Bohr hydrogen model; secondly, that the donor radii (determined via the position of the 1s–2p transition, within the Bohr model) directly correspond to the mean (Si, Al_{Si})–O bond lengths in the materials, for tetrahedra with mean Al content. This suggests that the donor is a simple point defect, possibly a lattice vacancy. Analysis of the OSL transitions for samples with bulk composition in the Na–Ca plagioclase feldspar series clearly shows that segregation is occurring on the submicroscopic scale into Na- and Ca-*richer* zones, but that the segregation into pure $NaAlSi_3O_8$ and $CaAl_2Si_2O_8$ crystal intergrowths (in analogy with the Na–K alkali feldspar series) is not complete.

It is finally noted that the work provides a possible explanation as to why similar infrared transitions are not observed in quartz. In the Bohr model, the IR transition in this material would be expected to occur at 0.86 eV (taking $m^* = 0.48m_e$ and $\epsilon_r = 2.38$ (Weinberg *et al* 1976, Deer *et al* 1992)), with an optical trap depth of 1.15 eV; charge trapped at such a centre would not be stable at room temperature.

Acknowledgments

This work is funded by Risø National Laboratory, the Department of Geology at Aarhus University, and the European Community under contract SCI-CT92-0800. It is also a pleasure to thank Professor J R Prescott for useful discussions, and the referees for their valuable comments and advice.

References

Aitken M J 1985 *Thermoluminescence Dating* (New York: Academic)
Baliff I K 1993 *Radiat. Prot. Dosim.* **47** 649–53
Bøtter-Jensen L, Ditlefsen C and Mejdahl V 1991 *Nucl. Tracks Radiat. Meas.* **18** 257–63
Bøtter-Jensen L, Duller G A T and Poolton N R J 1994a *Radiat. Meas.* **23** 613–6
Bøtter-Jensen L, Poolton N R J, Willumsen F and Christiansen H E 1994b *Radiat. Meas.* **23** 519–22
Clark R J and Sanderson D C W 1994 *Radiat. Meas.* **23** 641–6
Deer W A, Howie R A and Zussman J 1992 *An Introduction To The Rock Forming Minerals* 2nd edn (London: Longman Scientific and Technical)
Duller G A T 1991 *Nucl. Tracks Radiat. Meas.* **18** 371–8
Evseev Z Ya 1964 *Sov. Phys.–Solid State* **5** 1705–10
Fowler W B 1968 *Physics of Color Centers* ed W Beall Fowler (New York: Academic) ch 2
Hofmeister A M and Rossman G R 1985 *Phys. Chem. Miner.* **12** 324–32
Huntley D J, Godfrey-Smith D I and Haskell E H 1991 *Nucl. Tracks Radiat. Meas.* **18** 127–31
Huntley D J, McMullan W G, Godfrey-Smith D I and Thewalt M L W 1989 *J. Lumin.* **44** 41–6
Hütt G, Jaek I and Tchonka J 1988 *Quaternary Sci. Rev.* **7** 381–5
Kalniņš A, Pļaviņa I, Popov A I and Tāle A 1991 *J. Phys.: Condens. Matter* **3** 1265–70
Keller G V 1966 *Geol. Soc. Am. Mem.* **97** 552–77

Kittel C 1967 *Introduction To Solid State Physics* 3rd edn (New York: Wiley)
Kroll H and Ribbe P H 1983 *Rev. Mineralogy* **2** 57–99
Manning P G 1970 *Can. Min.* **10** 677–88
Prescott J R and Fox P J 1993 *J. Phys. D: Appl. Phys.* **26** 2245–54
Telfer D J and Walker G 1975 *Nature* **258** 694–5
—— 1978 *Mod. Geol.* **6** 199–210
Weinberg Z A, Johnson W C and Lampert M A 1976 *J. Appl. Phys.* **47** 248–55
Wintle A G 1993 *Radiat. Prot. Dosim.* **47** 627–35
Wright T L and Stewart D B 1968 *Am. Mineral.* **53** 38–87